1   VolKilau: **Vol**cano rapid response balloon campaign during the 2018 **Kilau**ea eruption

2   J.-P. Vernier[1,2], L. Kalnajs[3], J. A. Diaz[4], T. Reese[3], E. Corrales[4], and A. Alan [4], H. Vernier[5], L.

3   Holland[6], A. Patel[7], N. Rastogi[7], F. Wienhold[8] ,S. Carn[9] and N. Krotkov[10].

4   *1. National Institute of Aerospace, USA; 2. NASA Langley Research Center, USA; 3. Laboratory*

5   *for Atmospheric and Space Physics, University of Colorado at Boulder, USA; 4. GasLab.*

6   *CICANUM. Universidad de Costa Rica. San Jose, Costa Rica; 5. Virginia Institute of Marine*

7   *Science, Gloucester, USA. 6. University of Hawaii, USA; 7. Physical Research Laboratory,*

8   *India, 8. Swiss Federal Institute of Tech., Zurich, Switzerland, 9. Michigan Technological*

9   *University, Houghton, USA. 10. NASA Goddard Space Flight Center, USA.*

10   Corresponding author: Jean-Paul Vernier. E-mail : jeanpaul.vernier@nasa.gov

11   A Rapid balloon deployment during the 2018 Kilauea eruption provides a unique set of *in situ*

12   data to understand volcanic plume, chemical, and microphysical properties

13   **Abstract**

14   After nearly 35 years of stable activity, the Kilauea volcanic system in Hawaiʻi, went

15   through sudden changes in May 2018 with the emergence of 20 volcanic fissures along the

16   Lower Eastern Rift Zone (LERZ) destroying 700 homes in Leilani Estates and forcing more than

17   2000 people to evacuate. Volcanic emissions lasted for several months between June and

18   September 2018 leading to low visibility and poor air quality in Hawaiʻi and across the Western

19   Pacific. The NASA-funded VolKilau mission was rapidly mounted and conducted between 11-

20   18 June 2018 to: i) Profile volcanic emissions with SO_2 and aerosol measurements, ii) Validate

21   satellite observations and iii) Be prepared for the next large volcanic eruption. Through a series

of balloon-borne measurements with tethered and free released launches, we measured SO_2

concentration, aerosol concentration and optical properties 60 to 80 km downwind from the

volcanic fissures using gas sensors, optical particle counters, backscatter sondes, and an aerosol

impactor. While most of measurements made during the Kilauea eruption were ground-based,

the VolKilau mission represented a unique opportunity to characterize plume properties,

constrain emission profiles, study early chemistry involving the conversion of SO_2 into sulfuric

acid and understand the influence of water clouds in the removal of SO_2. Our team continues to

be better prepared for deploying in the event of a major volcanic eruption.

1. Introduction.

Volcanic eruptions have shaped life on the Earth through the combination of geologic

and atmospheric impacts. Major eruption can cool the climate system for several years (Robock

et al., 2000) from the veil of aerosols produced in the stratosphere (McCormick et al., 1995) that

reduces the amount of solar radiation reaching the surface. Tropospheric effusive eruption can

strongly deteriorate air quality with the release of sulfur-bearing gas and aerosols (Hansell et al.,

2004; 2006) and potentially affect the 450 million people worldwide living in proximity of

volcanoes (Small et al., 2001). The Laki eruption in 1783-84 led to an increase of mortality in

Iceland by >20% and devastating impacts on air quality and crop production throughout Europe

(Grattan et al., 2003; Witham and Oppenheimer, 2004). Cardiorespiratory and other acute health

effects have been observed on the people of Hawaiʻi from the recent eruptions of Kilauea (Longo

et al., 2013). Improving forecast system of dangerous life-threatening sulfur gases and

Particulate Matter (PM) is key to limit local population exposure. The complex physico-chemical

processes involved in the evolution of volcanic plumes from the few seconds after their

emissions start are not well understood. Observations of sulfate aerosols near volcanic sources

1   (Mather et al., 2003; Kroll et al., 2015) suggest rapid SO_2 oxidation and/or the production of

2   sulfate itself in the magma (Mather et al., 2003). Roberts et al. (2019) recently showed through

3   kinetic-based simulations that high temperature chemistry quickly forms oxidants such as OH,

4   HO_2 and H_2O_2 that can lead to the production of sulfate within a few second after the emission of

5   SO_2 starts. The aqueous pathways for sulfate formation have been studied with photochemical

6   model including isotope markers showing that TMI-O2 could indeed dominate the formation of

7   sulfate (Galeazzo et al., 2018) relative to other pathways through H_2O_2 and O_3, which can be

8   rapidly titrated at low pH. In addition, the production of sulfate through new particle formation

9   has been shown to be more frequent under the influence of volcanic emissions compared to

10   background level conditions (Rose et al., 2019, Boulon et al., 2011, Sahyoun et al., 2019).

11   Finally, halogen chemistry leading to ozone depletion has been observed in volcanic plumes

12   (Surl et al., 2015) that could affect oxidation processes. Therefore, measurements in fresh and

13   aged volcanic plumes are extremely important to understand the different pathways of SO_2

14   oxidation from OH in gas-phase and/or H_2O_2, O_3 and O_2 in liquid phase (Galeazzo et al., 2018).

15   Balloon-based measurements in fresh volcanic plumes are very limited but can provide

16   essential information on the vertical extension of SO_2 and aerosol concentration when the plumes

17   are lofted above the ground due to increased buoyancy. Pieri et al. (2013) reported one of the

18   first blimp and tethered balloon coincident observations of SO_2 and aerosol concentration at the

19   Turrialba volcano in Costa Rica to validate satellite observations from the Advanced Space

20   borne Thermal Emission and Reflection (ASTER). Balloon-borne measurements during the

21   Holuhraun eruption in Iceland (Vignelles et al., 2016) provided one of the first aerosol size

22   distribution of volcanic aerosols in very fresh lofted (age ~15 min) plume.

1   NASA Langley Research Center (LaRC) scientists teamed up with researchers from

2   Universities of Colorado and Costa Rica to rapidly deploy gas-aerosol-instrumented balloons

3   during the **Vol**cano rapid response balloon campaign during the **Kilau**ea eruption (VolKilau).

4   Through a series of 8 balloon flights in Hawaiʻi between June 11th and June 18th 2018, we

5   measured the atmospheric composition in the outflow plumes from the volcanic fissures and the

6   Halemaʻumaʻu main crater.

7   The purpose of this paper is to describe the preparation, the deployment and preliminary

8   results obtained during VolKilau. With SO_2 and aerosol measurements, we characterized the

9   Kilauea volcanic plumes with high vertical resolution balloon data. We show how our

10   measurements can be used to validate satellite observations and model dispersions and help shed

11   light on microphysical plume evolution.

12   2. The 2018 Kilauea eruption

13   2. a. Sudden geological changes of the Kilauea volcanic system

14   The state of Hawaii forms a chain of islands created over the last 60 million years through the

15   connection of a hotspot bringing magma from the inner mantle. Hawaiʻi is the youngest of the

16   archipelagos and Kilauea the most recent volcano which started to erupt 800 000 years ago. After

17   nearly 35 years of stable activity, in May 2018, the Kilauea volcano erupted from 20 new

18   fissures and sent lava flowing over streets and neighborhoods (Neal et al., 2019). Wiping out 700

19   homes and moving more than 2000 people, no US eruption was as disruptive since Mount St

20   Helens blew ash up to the stratosphere in 1980. The 2018 Kilauea eruption marked profound

21   changes of the volcanic system with the collapse of the Puʻu ʻŌʻō crater, the drain of the lava

22   lake of the Halemaʻumaʻu crater, also called Kilauea summit, and the emergence of volcanic

1   fissures along the Lower Eastern Rift Zone (LERZ) (Figure 1). Following a 6.9 magnitude

2   earthquake, volcanic fissures opened in the Leilani Estates area on May, 3rd and more than 20

3   fissures were reported the following weeks. The United States Geological Survey monitored the

4   extension of the lava fields through thermal Infrared camera mounted on helicopters (Neal et al.,

5   2019). In addition, NASA flew the Gulfstream III (G-III) to assess the volume of lava spilled out

6   by the volcanic fissures with a Synthetic Aperture Radar from the Jet Propulsion Laboratory.

7   Aside from lava destruction, volcanic fissures continuously emitted 30-60 kt of sulfur dioxide

8   (SO_2) in the atmosphere, which turned into sulfuric acid droplets forming the so-called volcanic

9   fog (vog) especially pronounced on the Southwestern side of the Island and over the Western

10   Pacific (Fig.3).

11   2. b. SO2 emissions during the Kilauea eruption

12

13   The first of the 20 volcanic fissures from the 2018 outbreak was observed on May 3rd in

14   the Leilani Estates area with levels of SO_2 threating air quality safety with violation of the

15   National Ambient Air Quality Standard for SO_2 and concentrations greater than 75 ppb. SO_2

16   emitted from the Kilauea summit and the LERZ have been measured daily by the Ozone

17   Mapping Profiling Suite (OMPS). OMPS nadir mapper is a hyperspectral ultraviolet

18   spectrometer (Flynn et al., 2014; Seftor et al., 2014) on board the NASA-NOAA National Polar

19   Partnership (NPP) satellite measuring SO_2 total vertical column density in Dobson Units (1 DU

20   $= 2.69 * 10^{16}$ SO_2 molecules per cm^2) using Principal Component Analysis (PCA) algorithm

21   (Zhang et al., 2017; Li et al., 2017). An assumed SO_2 profile shape, represented by its center of

22   Mass Altitude (CMA) near 2.5 km was used to derive the lower tropospheric (TRL) SO_2 map

23   shown in Fig.2 (top) (Ialongo et al., 2015). Figure 2 (bottom) shows a time series of total daily

1   mass of SO_2 (in kilotons: kt) between June and September 2018 (daily OMPS SO2 maps and

2   tonnages are available on-line at https://so2.gsfc.nasa.gov/pix/daily/0718/hawaii_0718p.html).

3   The Kilauea eruption lasted for 3 months between May and August 2018 (Fig.2) with a

4   maximum of 60 kt of SO_2 emitted on June 15th as inferred from OMPS. We note that this

5   estimate could be affected and underestimated several factors such as retrieval algorithm,

6   instrument resolution and the presence of clouds. The SO_2 plumes were transported by trade

7   winds and affected air quality across Hawai'i and Western Pacific (Fig.2/bottom).

8   During the 2018 eruption at Kilauea's LERZ, USGS reported SO_2 emissions over 30kt per day, a

9   value that could be affected by instrument saturation and wind speed assumptions

10   (https://www.usgs.gov/faqs/how-much-sulfur-dioxide-so2-gas-does-k-lauea-emit?qt-

11   news_science_products=0#qt-news_science_products). Figure 3 shows steam and gas emitted by the

12   volcanic cone produced by Fissure 8. The subsequent transformation of SO_2 into sulfate aerosols,

13   the vog is observed on a photo taken 20 km north from Kona on June, 10th. The large extension

14   of the vog is also evident on the true color image from the VIIRS/NPP on June, 7th characterized

15   by a grey-blueish veil observed hundreds of miles downwind from Hawai'i (Fig.3). While the

16   impacts of the Kilauea eruption on aviation was minimal, the vog presented a serious threat to air

17   quality across the Island and largely affected the tourist Industry (Neal et al., 2019).

18

19

20

21

22

1   3.   Campaign preparation and planning

2   Volcanic eruptions are by nature challenging to study. Being quasi-unpredictable and

3   sudden, scientists often rely on satellite observations to assess their atmospheric impacts.

4   Extreme conditions associated with volcanic eruptions make field measurements extremely

5   dangerous and thus rare. Finally, the composition of volcanic emissions, their dependency with

6   geological processes and the different stages of plume physico-chemical processing when

7   entering the atmosphere result in complex atmospheric impacts. Heat buoyancy created near

8   volcanic sources generate aloft plume that cannot always be captured by ground-based

9   measurements enhancing the value of airborne deployments.

10   Our team is involved with the NASA Disaster program (https://disasters.nasa.gov/kilauea-hawaii-

11   eruption-2018) and the Volcano Response (VolRes) international initiative to deploy during and

12   after volcanic eruptions. Within 15 days, VolKilau was on the ground of Hawaiʻi, nearly 60 km

13   downwind from fissures and 20 km from the Halemaʻumaʻu crater to study SO_2 and aerosol

14   emissions from the Kilauea eruption. We deployed a variety of balloon measurement payloads

15   just downwind from the eruptive vents to profile SO_2 and aerosol concentrations in the plume to

16   improve model simulations and validate satellite observations SO_2 and aerosols. We used

17   forecast maps of SO_2 provided by the University of Hawaii (Businger et al. 2015) to choose a

18   deployment location and sample the outflows of Kilauea emission zones. The NOAA Hybrid

19   Single Particle Lagrangian Integrated Trajectory (HYSPLIT) model (Draxler and Hess (1997);

20   Stein et al. 2015) was initialized between 50 and 700m above the local terrain to account for

21   buoyancy created at the emission sources. The volcanic plumes originated from three different

22   locations (Fissure 8 in the LERZ, Puʻu ʻŌʻō crater and Halemaʻumaʻu crater). Fissure 8 became

23   the largest source of SO_2 with flux between 30-60 kt/day a few weeks after the beginning of the

fissure outbreak, forming a volcanic cone (photo, Fig.3). The Puʻu ʻŌʻō crater, which rapidly

collapsed after the new fissures started erupting became a minor source. However, the Kilauea

summit occasionally produced ash clouds up to 10 000 ft and was an additional relatively small

source of SO_2 compared to Fissure 8.

After exploring several options remotely, it became obvious that choosing a location near the

Leilani Estates area could be dangerous given the potential high levels of SO_2 measured on the

ground at the proximity of the fissures but also complicated since the area was restricted to only

emergency responders and local people. The best option would become to deploy downwind

from the Fissure 8 where trade winds were pushing volcanic emissions toward us at acceptable

concentrations for outdoor activities. The Kapapala ranch (19.263, -155.445), located along road

11 between the Kapapala forest reserve and the Hawaiʻi Volcano national Park (See Fig.1)

became a viable option given past deployment experience of the team.

4. The VolKilau campaign

    a. Concept

The VolKilau campaign was designed to study the atmospheric outflow from the Kilauea

volcanic emissions with gas and aerosol measurements. The objectives of this mission were to i)

profile volcanic emissions, ii) validate satellite observations and iii) be prepared for the next

major volcanic eruption. The first and second objectives relied on obtaining vertically resolved

data of SO_2 and aerosols through the atmosphere. VolKilau was based on three types of

ballooning activities (Fig.4) : 1) Free released balloon to sample volcanic outflows from the

fissures but also high altitude ash cloud injected occasionally from the Kilauea summit, 2) Low-

level cut down balloon flight to optimize the measurements in the plume and terminate the flight

early for recovery and 3) Tethered balloon activities to sample the volcanic plume below 2 km.

1   b. Payloads

2 The payloads selected for the campaign measure SO_2 and aerosol optical, physical and chemical

3 properties. It included:

4 **LASP Light Weight OPC (ROPC)**: A lightweight and low-cost balloon borne optical particle

5 counter, based on a commercially available optical head (Met One 9722) integrated with a flow

6 control system and radio sonde telemetry system. This is the smallest of the balloon borne OPCs

7 developed at LASP and is well suited to measurements in the troposphere with relatively high

8 aerosol loadings. The size range in radius is between $0.15 - 5$ μm, with number concentration

9 ranging from $1 - 3x10^5$ #/l. The ROPC reaches a coincident counting threshold near 300 000

10 particles per liter. Above this limit, there is a statistically significant probability that more than

11 one particle may pass through the laser beam at one time, leading to an undercounting of

12 particles. While the instrument will still respond to particle concentrations above the coincidence

13 threshold, the measurement becomes qualitative in nature due to the increasing probability of

14 coincident particles. Mather et al. (2003) reported sulfate size distributions in the plume of the

15 Masaya volcano with a peak near 0.15 μm radius. Thus, our OPC measurements do not fully

16 capture the entire size distribution of sulfate and therefore likely provide lower limit estimates of

17 total aerosol number concentration.

18 **LOPC :** Another lightweight OPC developed at NASA Langley and adapted for weather balloon

19 flight applications, also using the MetOne 9722 particle counter with a small external pump from

20 *Particle Plus, Inc*. The data logging is based on Raspberry PI and is compatible with an Imet

21 meteorological radiosonde. The OPC includes 8 channels with sizes between $0.15 - 10$ μm and

22 the measurement range is similar to the ROPC.

COBALD is a lightweight (~500 g) balloon-borne backscatter sonde developed at the Institute

of Atmospheric and Climate Science, Swiss Federal Institute of Technology (ETH), Zurich.

COBALD consists of two high power (250 mW) Light Emitting Diodes (LEDs) which emit light

at 455 nm (blue) and 940 nm (near infrared) wavelengths. A silicon photo-diode placed between

the two LEDs collects the light backscattered from air-borne particles (molecules, aerosols and

clouds). When connected with an iMet radiosonde, the instrument transmits backscatter counts at

both of these wavelengths, pressure, temperature, relative humidity, wind speed and wind

direction at 1 Hz to the receiving ground station. The concurrent profiles of pressure, temperature

and backscattered counts are used to calculate Scattering Ratio (SR), the ratio of total

backscattering coefficient ($\beta = \beta_{p} + \beta_{m}$) to the molecular backscattering coefficient (β_{m}) at a

given wavelength. The ratio of (SR_{940}-1) at 940 nm to (SR_{455}-1) at 455 nm, defined as the color

index (CI), gives qualitative information about particle size (Cirisan et al., 2014; Vernier et al.,

2015).

MiniGAS system is an integrated suite of instruments for UAV applications including

meteorological (pressure, temperature) and up to 5 chemical sensors. The system uses a

microcomputer, a data logger and telemetry system from which gas concentrations can be

displayed in real time on a laptop (Diaz et al., 2015). The miniGAS PRO Version (Fig. 5) is

designed for volcanic gas measurements on small UAVs, multicopter drones and tethered

balloons/blimps for < 1.5km agl altitude flights. The miniGAS-PRO was deployed during the

2018 VolKilau campaign for measuring SO_2 concentration from the Kilauea volcanic plume. The

instrument collected SO_2 (0-20ppm range) and CO_2 (0-2000ppm range) on two tethered flights

coincidently with OPC measurements. SO_2 and CO_2 measurements are based on electrochemical

and Non Dispersive InfraRed (NDIR) techniques, respectively. A 0.2 μm PTFE teflon filter is

included at the entrance of the sensor to limit the intrusion of droplets inside the miniGAS and

affect the measurements. However, we cannot completely rule out potential measurement

artefacts at high relative humidity that may affect *in cloud* measurements.

Ozonesonde is a payload using the Electro Chemical Cell (ECC) measurement technique to

retrieve ozone concentration.

Ozone reacts with potassium iodide following: $2KI + O_3 + H_2O \rightarrow 2KOH + I_2 + O_2$ (1)

anode reaction: $3I^- \rightarrow I_3^- + 2e^-$ (2)

cathode reaction: $I_2 + 2e^- \rightarrow 2I^-$ (3) (exposed to ambient air and the presence of O_3)

However, SO_2 interferes with those measurements and reacts with water following the reaction*:*

$$SO_2 + 2H_2O \rightarrow 2e^- + SO_4^{2-} + 4H^+ \text{ (4)}$$

Each molecule of SO_2 produces 2 electrons, replenishing the cathode (3) and reducing the current

between the anode and the cathode. The interference of SO_2 has been used to infer SO_2 information

(Morisson et al., 2010) using one sonde with and without an SO_2 filter. With the DualSonde

technique, SO_2 is inferred by subtracting from the unfiltered signal (O_3+SO_2), the filtered signal

(O_3). During the campaign, we attempted to use the Dualsonde technique but quickly realized that

the levels of SO_2 were too high and led to the saturation of the signal. Thus, we used the

ozonesonde only has an indicator to find the bottom (during the ascent) and top (during the descent)

of the volcanic plume.

Impactor. Volcanic aerosol composition is investigated using an aerosol impactor, which was

initially prepared for tethered balloon applications but only run on the ground because of weight

limitations from Federal Aviation Authorities regulations and technical constrains. The MPS-3

Microanalysis Particle Sampler, a 3-stage impactor, was connected to a small air pump

delivering 1.4 lpm of flow and was run for 30 min to sample 42 l of air. Inertial impaction type

of sample collector is associated with particle size cut-points of 1.4 μm (Stage-1,S-1), 0.2 μm

(Stage-2, S-2) and down to 0.05 μm (Stage-3, S-3). After collection, the filters were placed in

2ml sterile polypropylene vials with deionized water (resistivity: 18.2 Ωcm^{-1}) and extracted for 3

intervals of 10 minutes each, by ultrasonication. The subsequent solutions were analyzed by ion

chromatography (DIONEX CS 5000) to detect water-soluble cations (Na^+, $NH4^+$, Mg^{2+}, K^+,

Ca^{2+}) and anions (Cl^-, NO_3^-. SO_4^{2-}, NO_2^-) using a cation column (DIONEX IonPac^{TM} CS16) and

anion column (DIONEX IonPac^{TM} AS23), coupled to their respective suppressors CERS/AERS

500, before the conductivity detector (Thermoscientific P/N 061830) (Patel and Rastogi, 2018).

c. Balloon Flights

The VolKilau campaign consisted of 8 balloon flights between June 11th and June 18th (table 1)

One flight took place from the Whittington Beach (19.086, -155.550) and the rest from the

Kapapala Ranch (19.263, -155,445). We launched 4 free-released, 4 tethered and one low-level

cut flights during this time frame. The trajectories of the free released balloon flights are shown

in Fig.6.

d. HYSPLIT trajectory model description

A custom version of the HYSPLIT model, referred to as the 'vog model', was run in real-time at

the University of Hawai'i at Mānoa to produce forecasts of SO_2 and sulfate aerosol (Businger et

al. 2015). The meteorological model input is a custom version of the Weather Research and

Forecasting – Advanced Research Weather (WRF-ARW) model with 900 m horizontal

resolution over the main Hawaiian Islands (Cherubini et al. 2008). The vog forecasts rely on

1   emission rates of SO_2 from the U.S. Geological Survey and Hawaiian Volcanoes Observatory.

2   Prior to the Lower East Rift Zone (LERZ) eruptive event, the vog model incorporated real-time

3   SO_2 emission estimates as weekly averages that were updated on a daily basis. These estimates

4   were made using a UV spectrometer array (Elias et al. 2018) and acted as the primary source

5   term for volcanic emissions in the vog model. The LERZ event interrupted operation of the UV

6   spectrometer array. Less frequent estimates made with mobile instrumentation were used instead

7   with DOAS UV spectrometer. The frequency of updates had a direct and notable impact on vog

8   model forecasts of concentrations (L. Holland et al., 2019, accepted).

9   5. Campaign preliminary results.

10   The VolKilau campaign dataset is analyzed together with satellite measurements of SO_2 and

11   aerosols, and simulations using the HYSPLIT trajectory model.

12   a. Free release flight into the Kilauea plume

13   After a tethered balloon test flight on June, 11th from the Kapapala Ranch, the first flight of the

14   campaign took place on June, 13th near 3am UTC with a combined flight with an Optical Particle

15   Counter (OPC) and an ECC for SO_2 information. Since SO_2 and wind forecasts showed that the

16   volcanic plume was further south than the Kapapala Ranch, we decided to move our equipment

17   along the shore of Hawaiʻi near the Whittington Beach (19.086, -155.549). Figure 7 shows

18   aerosol concentration profiles for r> 0.15 μm, 0.25 μm, 0.35 μm, 0.5 μm, 0 1 μm, 1.5 μm, 2.5

19   and 5 μm associated with Relative Humidity (RH) and temperature profiles. Corresponding true

20   color image from VIIRS as well as SO_2 lower tropospheric column map from OMPS instrument

21   3-4 h before the balloon flight are also shown. The SO_2 cloud is seen over Hawaiʻi and extending

22   further South-SouthWest across the Pacific Ocean. The true colored image shows a white cloud

1   (delineated by yellow contours) originating from Fissure 8. The ozone profile is shown to

2   decrease rapidly from 0.02 ppmv to negative values near 1.3 km high due to the presence of SO_2

3   , consistent with the base of the volcanic plume. To reduce SO_2 in the ECC cell, it takes time, so

4   the signal remain below 0 for a good portion of the flight, even though it was already out of the

5   Plume as indicated by the OPC data. Near 1.3 km, the aerosol concentration for r>0.15 µm

6   increases by a factor 10 within a few hundred meters, also indicating the base of the volcanic

7   plume. Volcanic aerosols are enhanced for all sizes when RH>100 % likely indicating the

8   presence of sulfate aerosol in saturated conditions. The volcanic cloud is observed between 1.5

9   and 3.5 km height with a maximum of concentration for r>0.15 micron near 2.5 km with values

10 reaching 3.10^5 #/l where the RH is below 100 %. Above saturation, aerosol concentration of r>5

11 µm peaks near 1.10^4 #/l (near 2.2 km), nearly 4 orders of magnitudes larger than at 2.5 km. The

12 wind direction (40-60°) trace back the 1.5-3.5 km layer to volcanic emissions from Fissure 8, 80

13 km away and wind speed (10-11m/s) indicates a plume age of ~2.2 h. Relative variations of

14 aerosol concentration in function of RH reveals potential interaction between volcanic aerosols

15 and water clouds. Saturated levels seem to favor the growth and dissolution of sulfate aerosols in

16 liquid water clouds with large sulfuric acid droplets while sub-saturated conditions generate

17 smaller particles likely through new particle formation (Rose et al., 2019, Boulon et al., 2011)

18 from photoxidation and the growth of sulfate aerosols from SO_2.

19   b. High Resolution OPC data

20 We conducted a low-level balloon flight (<5 km) using a radio-controlled cut down system to

21 sample the plume and terminate the flight to optimize the chance of recovery of the payloads.

22 This balloon flight was launched on June, 14th near 1am from the Kapapala Ranch downwind

23 from volcanic emissions of fissure 8 (Fig.8) and nearly 2h after an overpass of the MODerate

1   resolution Imaging radio Spectrometer (MODIS) on the Aqua satellite. The flight was terminated

2   at 5 km height but despite the accurate location of the landing; we could not recover the

3   payloads. The ascent and descent profiles (Fig.8) show high concentration of aerosols up to 3 km

4   like the previous day with the presence of larger aerosols within the cloud. The volcanic plume

5   is capped by a trade wind inversion at 2.9 km with dry air from the free troposphere above this

6   level. Wind speed within the layer between 4-9 m/s from 0-70°N is consistent with its origin

7   from fissure 8, 2-4 h prior to our measurements. While the optical particle counter was at the

8   coincidence counting limit throughout the plume ($3x10^5$ l^{-1}) from 1.2-2.9 km, the measurements

9   qualitatively show significant structure within in the plume with a series of ~100m thick layers

10 from 1.9 – 2.5km on ascent with significantly varying aerosol size distributions. After the flight

11 was remotely terminated, the instrument descended through the volcanic plume, re-entering the

12 plume approximately 2km north of the ascent profile. This descent profile shows a similar

13 overall vertical extent to the plume, but the structure within the plume is significantly different.

14 Throughout the descent the RH in the plume was greater than 100% probably causing the

15 majority of the aerosol to grow to radii above 1μm reducing the vertical structure within the

16 plume. The descent took place in a cloudy area as observed by MODIS (Fig.8) confirming the

17 presence of large water droplets as observed by the OPC. During the descent and below 2.5 km,

18 RH is blocked at 104% that may suggest instrument hysteresis issues in cloud interstitial

19 conditions. Both the internal structure observed during ascent profile and the differences between

20 the relatively closely spaced ascent and descent profiles reinforce the importance of considering

21 inhomogeneity within the plume as well as cloud/aerosol interactions.

22

23

1   c. Satellite comparison

2   One of the objectives of the VolKilau campaign was to compare and validate satellite

3   observation using our balloon data. A nearly coincident balloon flight was planned at 6am UTC

4   on June, 15th with a nearby overpass of the CALIPSO satellite (within 200 km and 6h)

5   downwind from fissure 8 and our balloon measurements. The measurements included an ECC, a

6   backscatter sonde (COBALD) and an Optical Particle Counter (OPC) shown in Figure 9. The

7   ECC saturated with high concentration of SO_2 (black dotted line near 1.2 km, Fig9b), thus the

8   unfiltered ECC data went to Zero coincidently with an increase of aerosol concentration. A

9   second aerosol layer is observed near 4-4.5 km on both aerosol instruments consistent with the

10   volcanic plume. Both layers are correlated with increasing RH between 40-95 % a consistent

11   with expected aerosol growth in humid environment as observed near the Etna volcano (Roberts

12   et al., 2018). Those moist layers very likely originate from fissure 8 with wind speed near 3-7

13   m/s coming from the 0-60°N direction, yielding a plume age near 2-5h. The CALIPSO overpass

14   200 km downwind and 6 h also indicate a double layer, one in the boundary layer capping at 3

15   km and in the free troposphere near 4 km. SO_2 and AOD maps from OMPS/NPP and

16   MODIS/Terra/Aqua also indicates the dispersion of the volcanic cloud westward downwind

17   from fissure 8, across the Western Pacific. CALIPSO intersected the volcanic plume associated

18   with high SO_2 and AOD from MODIS and OMPS and coincident with high backscatter values

19   and low depolarization (not shown) consistent with the presence of liquid sulfate aerosols for

20   both layers. Wind speed and direction near 4 km height observed on the balloon flight (6 m/s,

21   50-60 degree) are consistent with the movement of air masses moving South-Southeast and

22   crossing the CALIPSO overpass after 6h. Those measurements indicate that volcanic materials

23   from fissure 8 had a complex vertical and horizontal distribution depending on weather

1   conditions and atmospheric instability. Reports from USGS indicated convective cloud forming

2   above fissure 8 that could have transported volcanic materials up to the tropopause level.

3   However, no trace of volcanic aerosols above 5 km were observed by satellites or during the

4   VolKilau campaign. Nevertheless, those observations indicate that parts of Kilauea volcanic

5   plume were transported in the free troposphere above the Boundary Layer.

6   d. Volcanic plume chemical and microphysical changes.

7   Volcanic plume chemistry is investigated by combining temperature, RH, aerosols, SO_2 and

8   CO_{2}/SO_2 using a tethered balloon flight on June, 15th 2018 from the Kapapala Ranch (VK04).

9   The time series of those parameters between 23:16 and 23:45 UTC is shown in Figure 10

10 together with geolocation of the balloon flight on Google maps colored with SO_2 measurements.

11 Levels of SO_2 near the surface were approaching 0.3 ppmv and increased up to 0.5 ppmv at

12 23:31 just before entering a water cloud near 1 km asl as indicated by RH near 100% and a

13 sudden increase of particle concentrations for sizes between 0.5 to 10 µm. The tethered balloon

14 was brought down after encountering the clouds since FAA regulations required a continuous

15 sight of view with the balloon during those activities. Outside the water cloud, the RH dropped to

16 70% and SO_2 levels regain their levels near 0.5 ppmv while the concentration of aerosols

17 dropped. CO_2 concentration is nearly constant within the plume so that the increase of CO_{2}/SO_2

18 ratio observed in Fig.10 is driven by the sharp drop of SO_2 and likely suggest the absence of SO_2

19 within clouds. However, we cannot exclude that cloud droplets affected the miniGAS

20 measurements despite the presence of a PTFE filter at the entrance to prevent the intrusion of

21 sulfuric acid droplets. Coincident measurements of SO_2 and aerosols near the vent of volcano

22 likely reveal the interaction between water vapor, SO_2 and aerosols (Roberts et al., 2018). *In-*

23 *cloud* SO_2 decreased rapidly probably because of different aqueous pathways leading to the

1 formation of sulfate either from the oxidation of H_2O_2 (Carn et al., 2011), O_3 and/or the TMI-O2

2 pathway (Galeazzo et al., 2018) even if we cannot rule out potential measurement artifacts of

3 SO_2 in high RH conditions. The vog was observed downwind form Fissure 8 across the Pacific

4 Ocean.

5   e. Volcanic aerosol composition

6 Volcanic composition is investigated using an aerosol impactor. We show the ionic composition

7 of two samples, HS1(Hawai'i Sample 1) and HS2(Hawai'i Sample 2) collected on June 12th and

8 14th 2018 at 5.30 am and 7.44am for 30 min with a flow of 1.4 lpm for a total of 42 l of air

9 sampled. Stage 1 and 2 for the two set of samples hold similar concentration of major ions in

10 aerosols between 3950 and 5900 ng/m3. Here, Na^+ and Cl^- ions dominate the total ionic mass

11 with a smaller contribution of $SO4^{2-}$ in stage 1 (r>1.4 µm) and stage 2 (1.4 µm <r<0.05 µm). The

12 major difference observed between the two samples is on stage 3 (r≤ 0.05 µm) where the

13 concentration of $SO4^{2-}$ and NH_4^+ aerosols are 6.2 and 7.9 times, respectively, higher in HS2

14 compared to HS1 (Fig. 11). Those measurements are compared with HYSPLIT simulations at

15 the time of the collections. HYSPLIT also shows much larger concentration of SO_2 (by a factor

16 of 2 to 10) during HS2 compared to HS1 consistent with favorable meteorological conditions

17 bringing volcanic material toward the measurement on June 14th compare to June 12th when trade

18 winds pushed volcanic aerosols offshore. Further, Cl^-/Na^+ ratios on stages 1 and 2 of samples

19 HS1 and HS2 were similar to their sea-salt ratio (1.8); however, on stage 3 it was about 3.3 i.e.,

20 ~2 times higher than expected from sea-salts. This observation suggests the presence of excess

21 Cl^- on the stage 3 in both the samples. Relatively high Cl^- on stage 3 indicates likely a significant

22 contribution of Cl^- from volcanic emissions resulting from the hydrochloric acid emissions from

23 lava entering the ocean (Resing et al., 1999). Further, non-sea-salt (nss) fraction of $SO4^{2-}$,

estimated using SO_4^{2-}/Na^+ ratio in sea-salt as a reference, was low on stages 1 and 2 but close to 100% on stage 3. We note also the presence of NH_4^+ on stage 3 of HS1 and HS2 bearing somewhat similar relative concentration with non-sea-salt (nss)-SO_4^{2-}, indicating the presence of SO_4^{2-} aerosol in the form of $(NH_4)_2SO_4$. While the presence of SO_4^{2-} is consistent with the rapid conversion of SO_2 into sulfate aerosols in the troposphere, its apparent association with NH_4^+ is interesting. The neutralization of acidic volcanic sulfate by ammonia has already been observed after the 2011 Grimsvötn volcano 3000 km from the sources. This process is size dependent with the neutralization efficiency enhanced for small particles (Šakalys et al., 2016). Our results also suggest that the neutralization of sulfate near the ground was dominant for particles smaller than 50 nm diameter. However, the level of neutralization was much larger than those found by Kroll et al. (2015) which reported a ratio SO_4^{2-}/NH_4^+ between 10-20 at Pahala less than 10 km away from our measurement site. The proximity of livestock could eventually explained the enhance levels of neutralization. However, a significant fraction of SO_4^{2-} was present as free acid as indicated by observed mass ratio of sulfate/ammonium (3.6) in comparison to expected mass ratio (2.7) if all sulfate would have existed as $(NH_4)_2SO_4$.

6. Conclusion

The 2018 Kilauea eruption was the most significant volcanic event in the US since Mt St Helen erupted almost 4 decades ago. Our team deployed quickly in Hawai'i to i) obtain vertically resolved profiles of SO_2, aerosol and meteorological parameters, ii) validate satellite observations and iii) be better prepared for the next large volcanic eruption. We deployed within 15 days in Hawai'i between June 11th and June 18th 2018 with 8 flights through tethered-, low-level cut and free released balloon activities from a Ranch downwind from active volcanic fissures and the Kilauea main crater. We flew multiple times in the volcanic plume from Fissure

1 8 emissions and found aerosol number concentration up to 3×10^5 #/l. Coincident measurements

2 between SO_2, aerosol concentration and RH suggest rapid conversion of SO_2 into aerosols in

3 supersaturated conditions leading to the formation of the vog. Satellite observations and balloon

4 data demonstrates the complexity of volcanic emissions with multiple volcanic layer observed up

5 to 4.5-5 km asl in the free troposphere. Finally, chemical analysis of ground-based samples

6 shows the recurrent presence of Sea Salt (NaCl) together with volcanic sulfate. The mass

7 concentration of sulfate can vary by a factor of 6 within a few days depending on wind

8 conditions as revealed by HYSPLIT simulations. Excess of Cl^- relative to the Cl^-/Na^+ ratio of

9 sea salt reveals the influence of hydrochloric acid emissions from lava entering the ocean

10 (Resing et al., 1999). The presence of ammonium in the samples suggest that acidic volcanic

11 sulfate are rapidly neutralized with the ammonia released by livestocks, which were at the

12 proximity of the measurement location. The VolKilau mission represented a unique opportunity

13 to combined SO_2 and aerosol measurements to understand aerosol microphysics in the Kilauea

14 volcanic plume. We tested instruments in the tropospheric volcanic plume environment so that

15 they can be used during future large volcanic eruptions.

16

17

18

19

20

21

7

8

9

10

11

12

13

14

15

16

17

18

19

7. References

Boulon, J., Sellegri, K., Hervo, M., & Laj, P. (2011). Observations of nucleation of new particles in a volcanic plume. *Proceedings of the National Academy of Sciences*, *108*(30), 12223 LP – 12226. https://doi.org/10.1073/pnas.1104923108

Businger, S., R. Huff, K. Horton, A. J. Sutton and T. Elias, 2015: Observing and Forecasting Vog Dispersion from Kīlauea Volcano, Hawai'i. Bull. Amer. Met. Soc., 96, 1667-1686. doi:10.1175/BAMS-D-14-00150.1.

Carn, S. A., et al. (2011), In situ measurements of tropospheric volcanic plumes in Ecuador and Colombia during TC4, *Geophys. Res. Lett.*, **116**, D00J24, doi:10.1029/2010JD014718.

Cherubini, T., S. Businger, R. Lyman, and M. Chun, 2008: Modeling Optical Turbulence and Seeing over Mauna Kea. *J. Appl. Meteor. Clim.*, 47, 1140-1155.

Cirisan, A., Luo, B. P., Engel, I., Wienhold, F. G., Sprenger, M., Krieger, U. K., et al. (2014). Balloon-borne match measurements of midlatitude cirrus clouds. *Atmospheric Chemistry and Physics*, *14*(14), 7341–7365. https://doi.org/10.5194/acp-14-7341-2014

Diaz J.A., Pieri D., Wright K., Sorensen P., Kline-Shoder R., Arkin CR., Fladeland M., Bland G., Buongiorno M.F., Ramirez C., Corrales E., Alan A., Alegria O., Diaz D. and Linick J., (2015) *"Unmanned aerial mass spectrometer systems for in-situ volcanic plume analysis"*. J Am Soc Mass Spectrom. 26(2): 292-304. Jan 2015. DOI: 10.1007/s13361-014-1058-x

Draxler, R., and G. D. Hess, 1997: Description of the HYSPLIT_4 modelling system. NOAA Tech. Memo. ERL ARL-224, 27 pp.'

Elias, T., C. Kern, K. Horton, A. Sutton, and H. Garbeil, 2018: Measuring SO2 Emission Rates at Kīlauea Volcano, Hawaii, Using an Array of Upward-Looking UV Spectrometers, 2014–2017. *Frontiers in Sci.*, 6, 214.

Hansell, A., & Oppenheimer, C. (2004). Health Hazards from Volcanic Gases: A Systematic Literature Review. *Archives of Environmental Health: An International Journal*, *59*(12), 628–639. https://doi.org/10.1080/00039890409602947

Hansell, A., Horwell, C., & Oppenheimer, C. (2006). The health hazards of volcanoes and geothermal areas. *Occupational and Environmental Medicine*, *63*, 125,149-156. https://doi.org/10.1136/oem.2005.022459

Flynn, L., Long, C., Wu, X., Evans, R., Beck, C. T., Petropavlovskikh, I., McConville, G., Yu, W., Zhang, Z., Niu, J., Beach, E., Hao, Y., Pan, C., Sen, B., Novicki, M., Zhou, S. and Seftor, C.: Performance of the Ozone Mapping and Profiler Suite (OMPS) products, J. Geophys. Res. Atmos., 119(10), 6181–6195, doi:10.1002/2013JD020467, 2014.

Galeazzo, T., Bekki, S., Martin, E., Savarino, J., & Arnold, S. R. (2018). Photochemical box modelling of volcanic SO2 oxidation: Isotopic constraints. *Atmospheric Chemistry and Physics*, *18*(24), 17909–17931. https://doi.org/10.5194/acp-18-17909-2018

Grattan, J., Durand, M., & Taylor, S. (2003). Illness and elevated Human Mortality in Europe Coincident with the Laki Fissure eruption. *Geological Society London Special Publications*, *213*. https://doi.org/10.1144/GSL.SP.2003.213.01.24

Ialongo, I., Hakkarainen, J., Kivi, R., Anttila, P., Krotkov, N. A., Yang, K., Li, C., Tukiainen, S., Hassinen, S., and Tamminen, J.: Comparison of operational satellite SO$_2$ products with ground-based observations in northern Finland during the Icelandic Holuhraun fissure eruption, Atmos. Meas. Tech., 8, 2279–2289, https://doi.org/10.5194/amt-8-2279-2015, 2015.

Kroll, J. H., Cross, E. S., Hunter, J. F., Pai, S., Wallace, L. M. M., Croteau, P. L., … Frankel, S. L. (2015). Atmospheric Evolution of Sulfur Emissions from Kīlauea: Real-Time Measurements of Oxidation, Dilution, and Neutralization within a Volcanic Plume. *Environmental Science & Technology*, *49*(7), 4129–4137. https://doi.org/10.1021/es506119x.

Holland, L., Businger, S., Elias, T., and Cherubini, T.: Two Ensemble Approaches for Forecasting Sulfur Dioxide Concentrations From Kīlauea Volcano. Weather and Forecasting, accepted, 2019.

Li, C., Krotkov, N. A., Zhang, Y., Leonard, P., Joiner, J., OMPS/NPP PCA SO2 Total Column 1-Orbit L2 Swath 50x50km V1, Greenbelt, MD, USA, Goddard Earth Sciences Data and

Information Services Center (GES DISC), Accessed: 15 June 2019, https://doi.org/10.5067/MEASURES/SO2/DATA203, 2017.

Longo, B. M., "Adverse Health Effects Associated with Increased Activity at Kīlauea Volcano: A Repeated Population-Based Survey," ISRN Public Health, vol. 2013, Article ID 475962, 10 pages, 2013. https://doi.org/10.1155/2013/475962.

Patel, A., Rastogi, N., 2018. Oxidative potential of ambient fine aerosol over a semiurban site in the Indo-Gangetic Plain. Atmos. Environ. 175, 127–134.

Mather, T. A., A. G. Allen, C. Oppenheimer, D. M. Pyle, and A. J. S. McGonigle (2003), Size-resolved characterisation of soluble ions in the particles in the tropospheric plume of Masaya volcano, Nicaragua: Origins and plume processing, *J. Atmos. Chem.*, **46**, 207– 237.

McCormick, M. P., Thomason, L. W., & Trepte, C. R. (1995). Atmospheric effects of the Mt Pinatubo eruption. *Nature*, *373*(6513), 399–404. https://doi.org/10.1038/373399a0

Morrison, G.A., Komhyr, W.D., Hirokawa, J., *et al.* (2010). A Balloon Sounding Technique for Measuring SO_2 Plumes. *Journal of Atmospheric and Oceanic Technology, 27*, 1318-1330.

Neal, C. A., Brantley, S. R., Antolik, L., Babb, J. L., Burgess, M., Calles, K. Cappos, M., Chang, J. C., Conway, S., Desmither, L., Dotray, P., Elias, T., Fukunaga, P., Fuke, S., Johanson, I. A., Kamibayashi, K., Kauahikaua, J., Lee, R. L. (2019). The 2018 rift eruption and summit collapse of Kilauea Volcano. *Science*, **363**, 367– 374. https://doi.org/10.1126/science.aav7046

Pieri, D., Diaz, J., Bland, G., Fladeland, M., Madrigal, Y., Corrales, E., … Abtahi, A. (2013). In situ observations and sampling of volcanic emissions with NASA and UCR unmanned aircraft, including a case study at Turrialba Volcano, Costa Rica. *Geological Society of London Special Publications*, *380*, 321–352. https://doi.org/10.1144/SP380.13

Resing, J. A., & Sansone, F. J. (1999). The chemistry of lava–seawater interactions: the generation of acidity. *Geochimica et Cosmochimica Acta*, *63*(15), 2183–2198. https://doi.org/https://doi.org/10.1016/S0016-7037(99)00193-3.

Roberts, T. J., Vignelles, D., Liuzzo, M., Giudice, G., Aiuppa, A., Coltelli, M., et al. (2018). The primary volcanic aerosol emission from Mt Etna: size-resolved particles with SO2 and

role in plume reactive halogen chemistry. *Geochim. Cosmochim. Acta* 222, 74–93. doi: 10.1016/j.gca.2017.09.040

Robert, T., Dayma, G., and Oppenheimer, C.: Reaction rates control high-temperature chemistry of volcanic gases in air, Front. Earth Sci., 7, 154, https://doi.org/10.3389/feart.2019.00154, 2019

Robock, A. (2000). Volcanic eruptions and climate. *Reviews of Geophysics*, *38*(2), 191–219. https://doi.org/10.1029/1998RG000054

Rose, C., Foucart, B., Picard, D., Colomb, A., Metzger, J. M., Tulet, P., & Sellegri, K. (2019). New particle formation in the volcanic eruption plume of the Piton de la Fournaise: Specific features from a long-term dataset. *Atmospheric Chemistry and Physics*, *19*(20), 13243–13265. https://doi.org/10.5194/acp-19-13243-2019.Šakalys, J. , E. meinorė, and K. Kvietkus. Neutralization of acidic sulfates with ammonia in volcanic origin aerosol particles Lithuanian Journal of Physics, Vol. 56, No. 1, pp. 42–48 (2016).

Sahyoun, M., Freney, E., Brito, J., Duplissy, J., Gouhier, M., Colomb, A., … Sellegri, K. (2019). Evidence of New Particle Formation Within Etna and Stromboli Volcanic Plumes and Its Parameterization From Airborne In Situ Measurements. *Journal of Geophysical Research: Atmospheres*, *124*(10), 5650–5668. https://doi.org/10.1029/2018JD028882.

Seftor, C. J., Jaross, G., Kowitt, M., Haken, M., Li, J. and Flynn, L. E.: Postlaunch performance of the Suomi National Polar-orbiting Partnership Ozone Mapping and Profiler Suite (OMPS) nadir sensors, J. Geophys. Res. Atmos., 119(7), 4413–4428, doi:10.1002/2013JD020472, 2014

Small, C., & Naumann, T. (2001). The global distribution of human population and recent volcanism. *Global Environmental Change Part B: Environmental Hazards*, *3*(3), 93–109. https://doi.org/https://doi.org/10.1016/S1464-2867(02)00002-5

Stein, A.F., Draxler, R.R., Rolph, G.D., Stunder, B.J.B., Cohen, M.D., Ngan, F., 2015. NOAA's HYSPLIT atmospheric transport and dispersion modeling system. Bull. Amer. Meteor. Soc. 96, 2059–2077. https://doi.org/10.1175/BAMS-D-14-00110.1

Surl, L., Donohoue, D., Aiuppa, A., Bobrowski, N., & Von Glasow, R. (2015). Quantification of the depletion of ozone in the plume of Mount Etna. *Atmospheric Chemistry and Physics*,

15(5), 2613–2628. https://doi.org/10.5194/acp-15-2613-2015

Vernier, J.-P., Fairlie, T. D., Natarajan, M., Wienhold, F. G., Bian, J., Martinsson, B. G., et al. (2015). Increase in upper tropospheric and lower stratospheric aerosol levels and its potential connection with Asian pollution. *Journal of Geophysical Research: Atmospheres*,*120*(4), 1608–1619. https://doi.org/10.1002/2014JD022372.

Vernier, J.-P., Fairlie, T. D., Deshler, T., Venkat Ratnam, M., Gadhavi, H., Kumar, B. S., … Renard, J.-B. (2018). BATAL: The balloon measurement campaigns of the Asian tropopause aerosol layer. *Bulletin of the American Meteorological Society*, *99*(5). https://doi.org/10.1175/BAMS-D-17-0014.1.

Vignelles, D, Roberts, TJ, Carboni, E et al. 2016. *Balloon-borne measurement of the aerosol size distribution from an Icelandic flood basalt eruption.* Earth and Planetary Science Letters, 453. pp. 252-259. ISSN 0012-821X.

Witham, C., & Oppenheimer, C. (2004). Mortality in England during the 1783-4 Laki Craters eruption. *Bulletin of Volcanology*, *67*, 15–26. https://doi.org/10.1007/s00445-004-0357-7

Zhang, Y., C. Li, N. A. Krotkov, J. Joiner, V. Fioletov, and C. McLinden (2017), Continuation of long-term global SO_2 pollution monitoring from OMI to OMPS, *Atmos. Meas. Tech.*, 10,

1   8. Figures
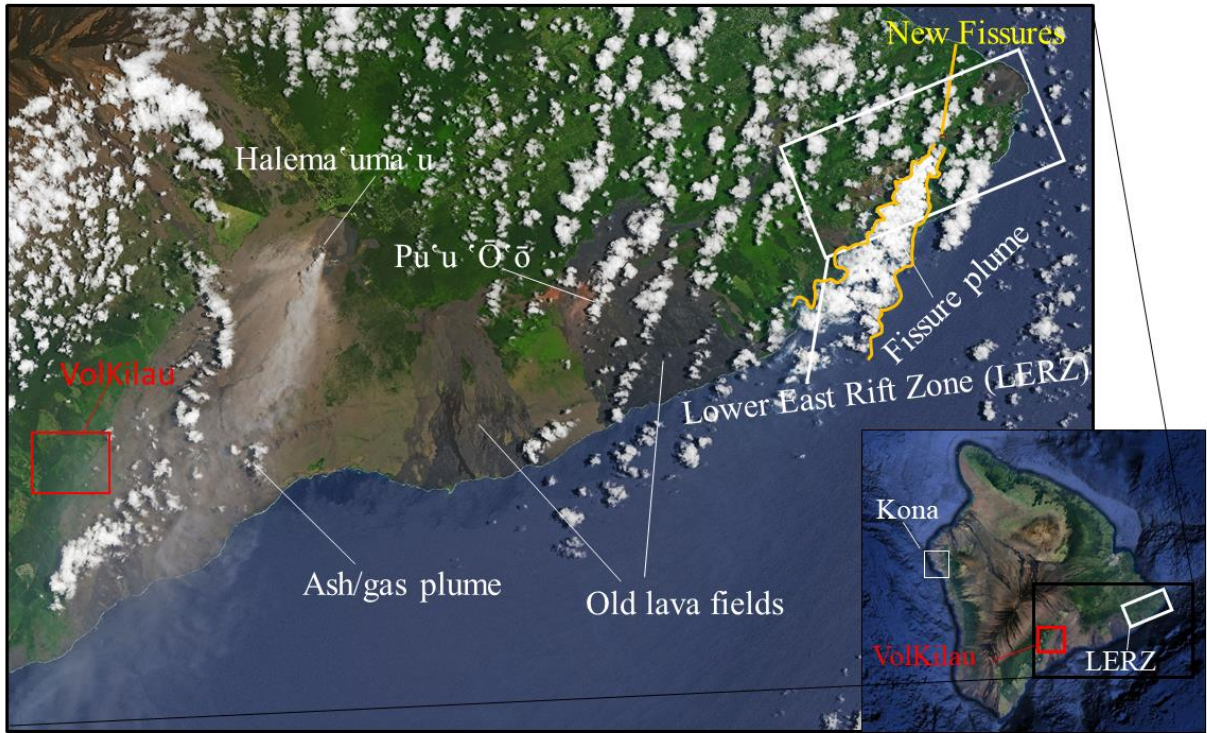
2   9.

3   *Figure 1. True Color image from the NASA/USGS Landsat 8 Operational Land Imager on May,*

4   *14th 2018 in south Hawaiʻi. The Puʻu ʻŌʻō crater, Halemaʻumaʻu summit, Lower East Rift Zone*

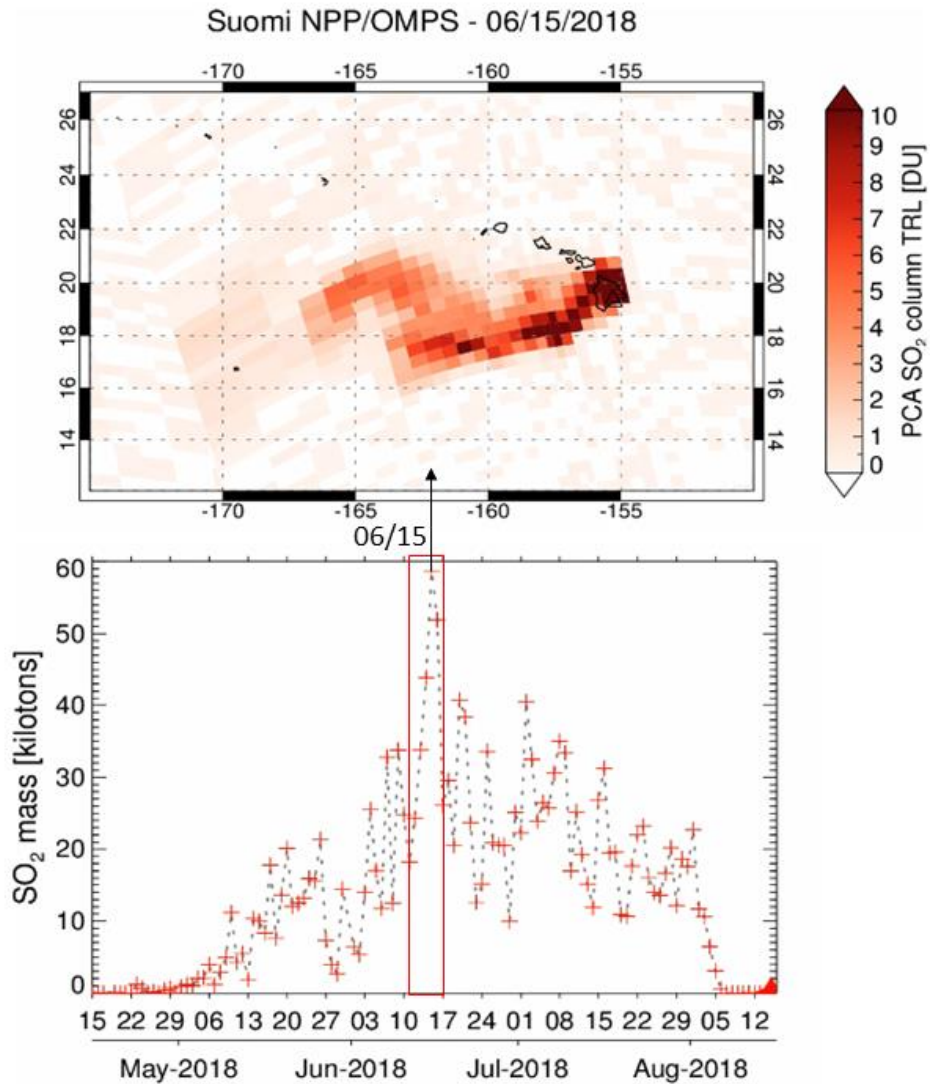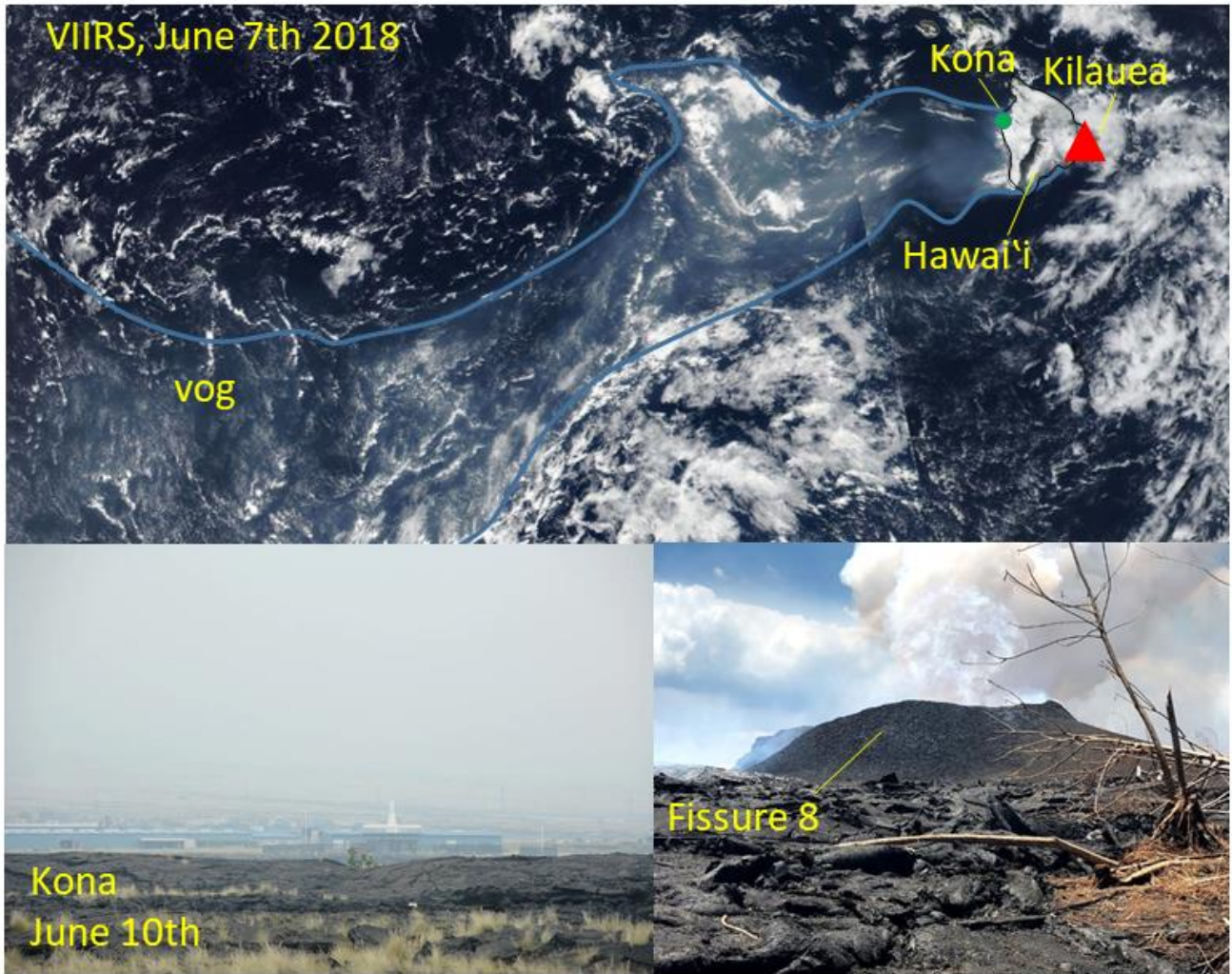5   *(LERZ) and the location of the VolKilau campaign are shown.*

6

7

8

9

10

11

1

Figure 2. (Bottom) Time series of SO_2 mass (in kilotons) from OMPS/NPP nadir mapper during

the 2018 Kilauea eruption and (top) map of lower tropospheric (TRL) SO_2 on June 15th 2018

using the Principal Component Analysis (PCA) algorithm.

5

6

7

1

2

3 *Figure 3. (Top) True color image shows the vog across the Western Pacific observed by*

4 *VIIRS/NPP on June, 7th 2019. (Bottom) photos of the vog in Kona on June, 10th and volcanic*

5 *emissions from fissure 8 on June, 18th (photo credit. J-P. Vernier).*

6

7

8

1
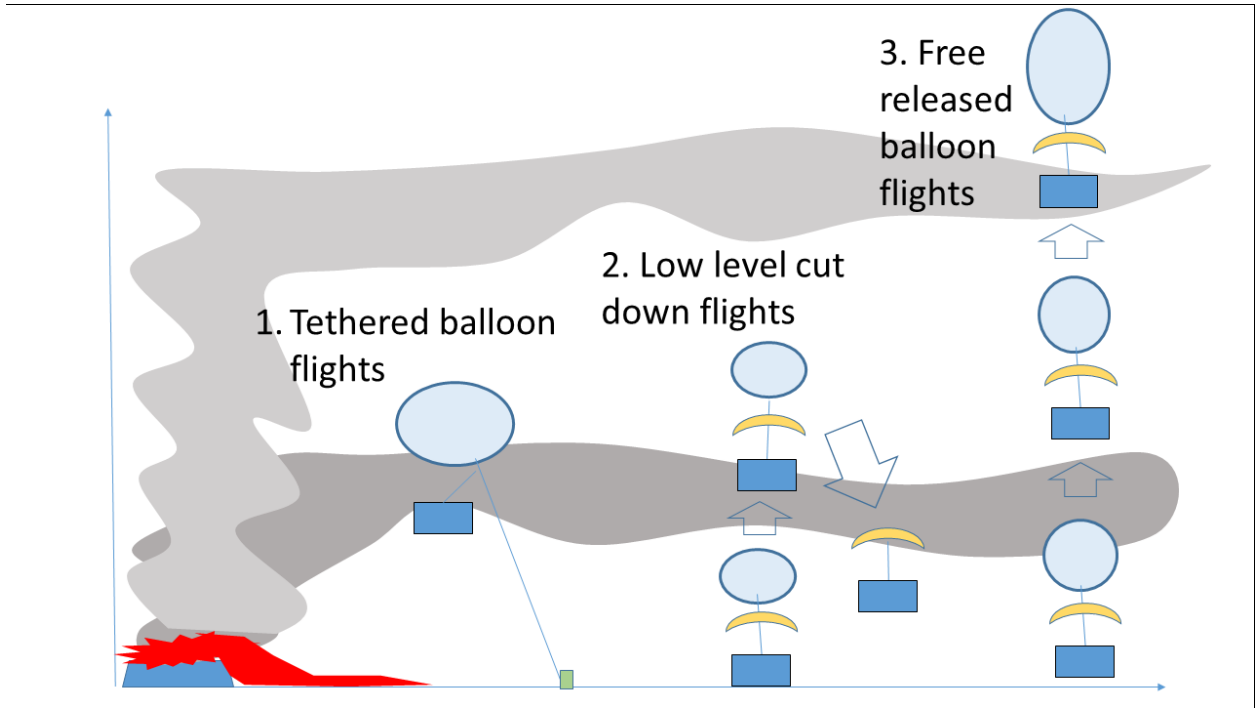
2

3   *Figure 4. Balloon activities during the VolKilau campaign to sample volcanic plumes emitted at*

4   *low altitudes from the fissures in the LERZ and at higher levels from explosive events at the*

5   *Kilauea summit.*

6

7

8

9

10

11

12

13

1
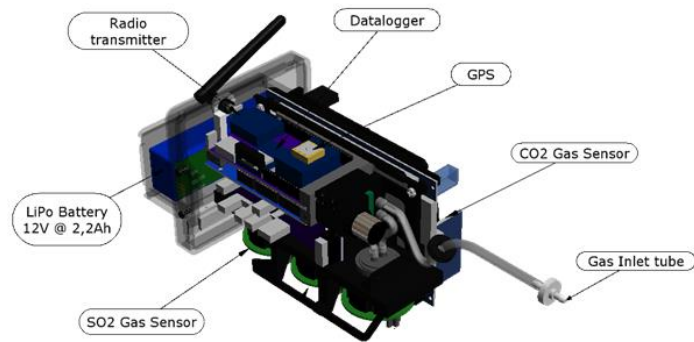
2

3 *Figure 5. Schematic and picture of the miniGAS PRO, a 1.5kg miniature multiple gas payload*

4 *which incorporates waterproof case, GPS, SO_2 and CO_2, temperature and relative humidity*

5 *sensors with onboard datalogger and telemetry, designed for UAV/ drone or tethered*

6 *balloon/blimp measurements.*

7

8

9

1
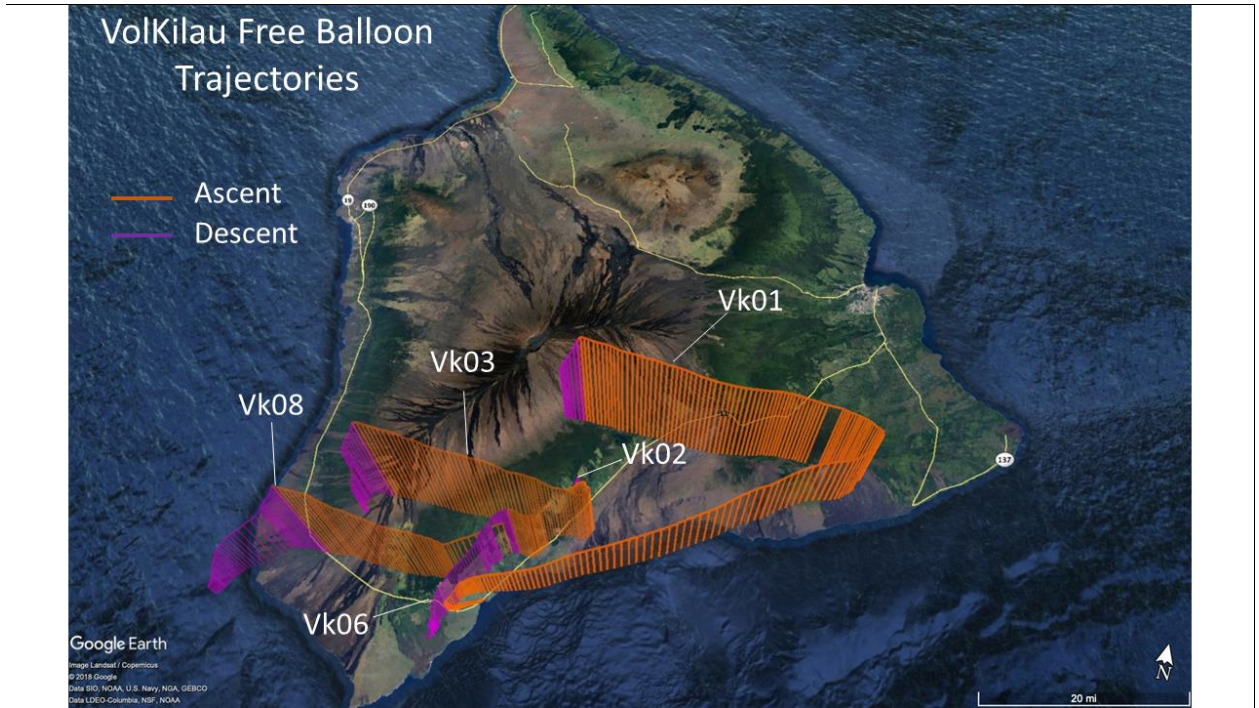
2

3   *Figure 6. Trajectories of the 5 free released balloon flights during the VolKilau campaign.*

4   *Balloon ascent is shown in orange and descent in magenta.*
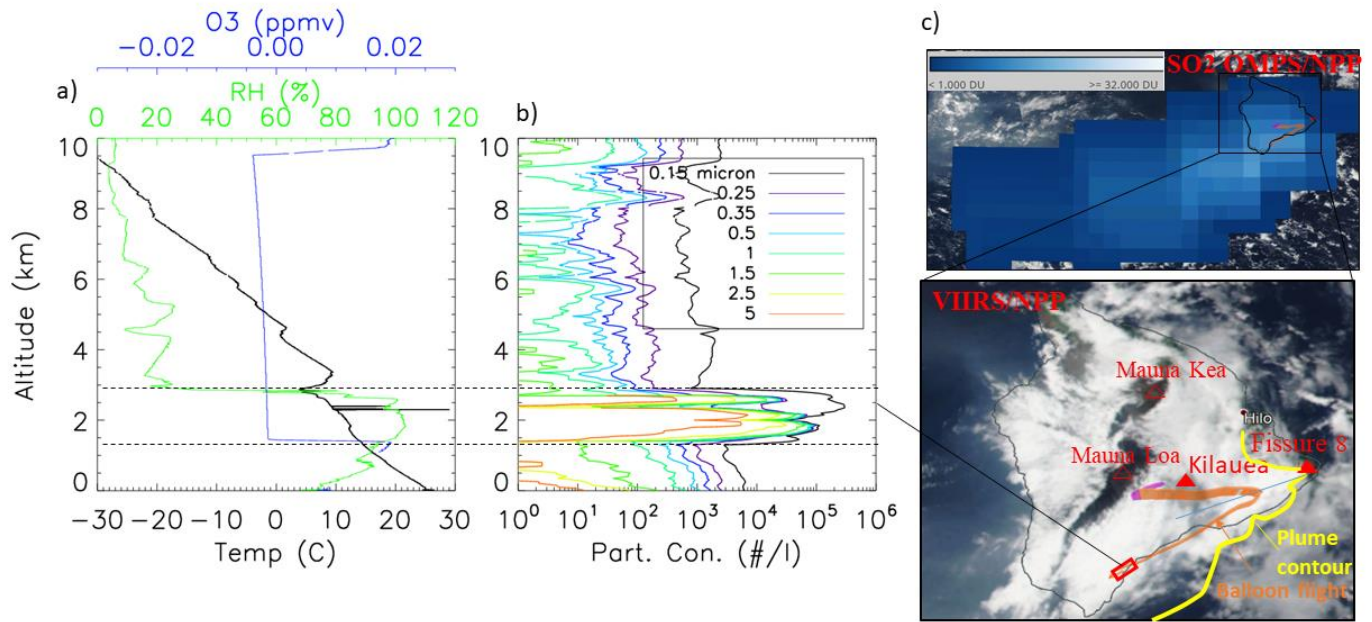
5

6

7

8

9

10

11

12

1

2

3   *Figure 7. Data from a free-released balloon flight launched on June, 13th 2018 near 3am (UTC)*

4   *from the Whittington beach (19.086, -155.550). Profiles of (a) temperature, Relative Humidity*

5   *(RH), ozone mixing ratio, and (b) aerosol concentration profiles for r(radius)>0.15μm,*

6   *r>0.25μm, r>0.35μm, r>0.5μm, r>1 μm, r>1.5μm, r>2.5μm and r>5μm. (c) Corresponding*

7   *SO_2 lower tropospheric column map from OMPS/NPP (top) and true color image from*

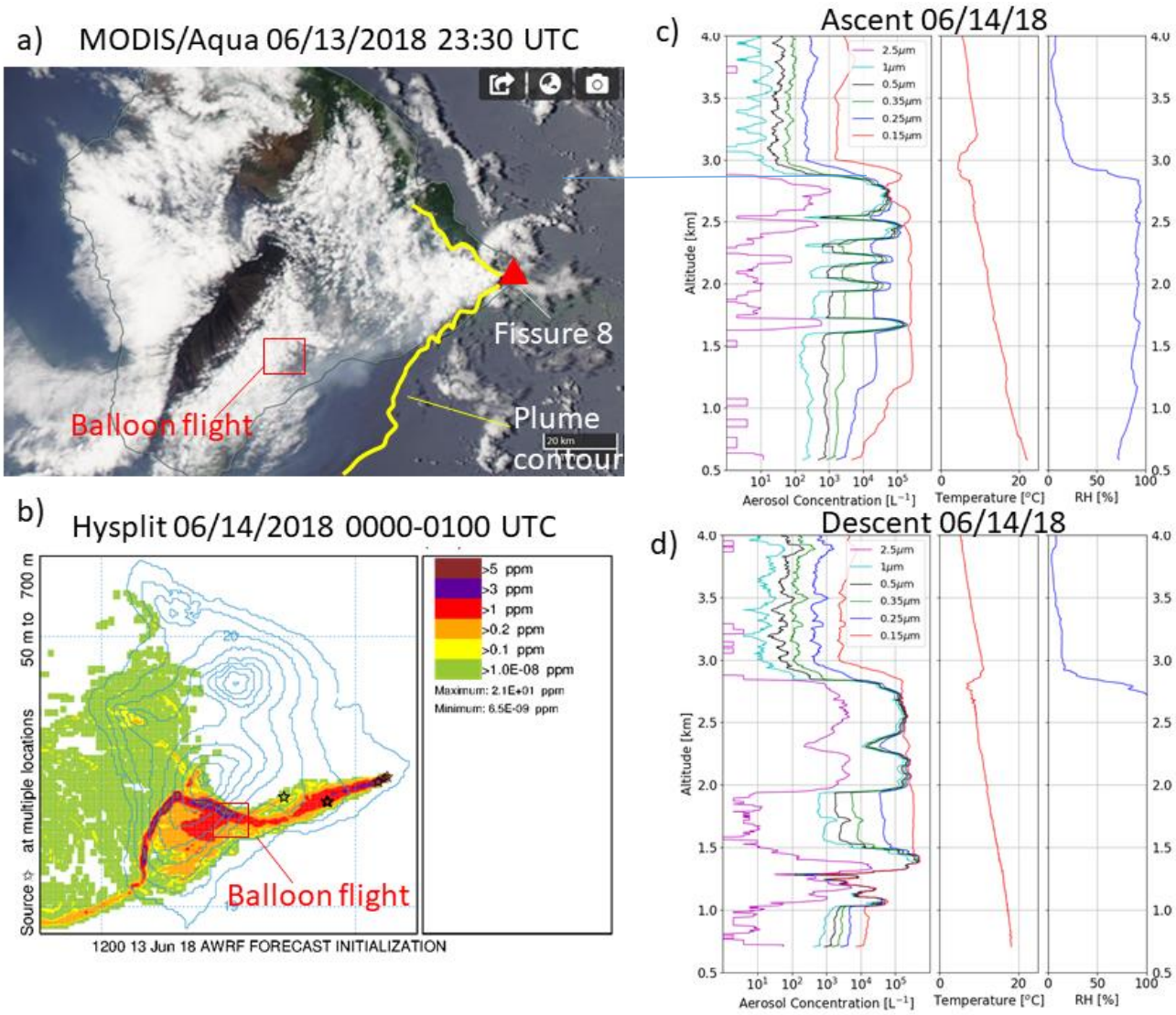8   *VIIRS/NPP near 23UTC on June, 12th superimposed with balloon flight trajectory (bottom).*

9   *Volcanic plume emitted from fissure 8 in the LERZ is drawn with a yellow contour.*

10

11

12

13

1

Figure 8. (a) True color image from the MODerate resolution Imaging radioSpectrometer

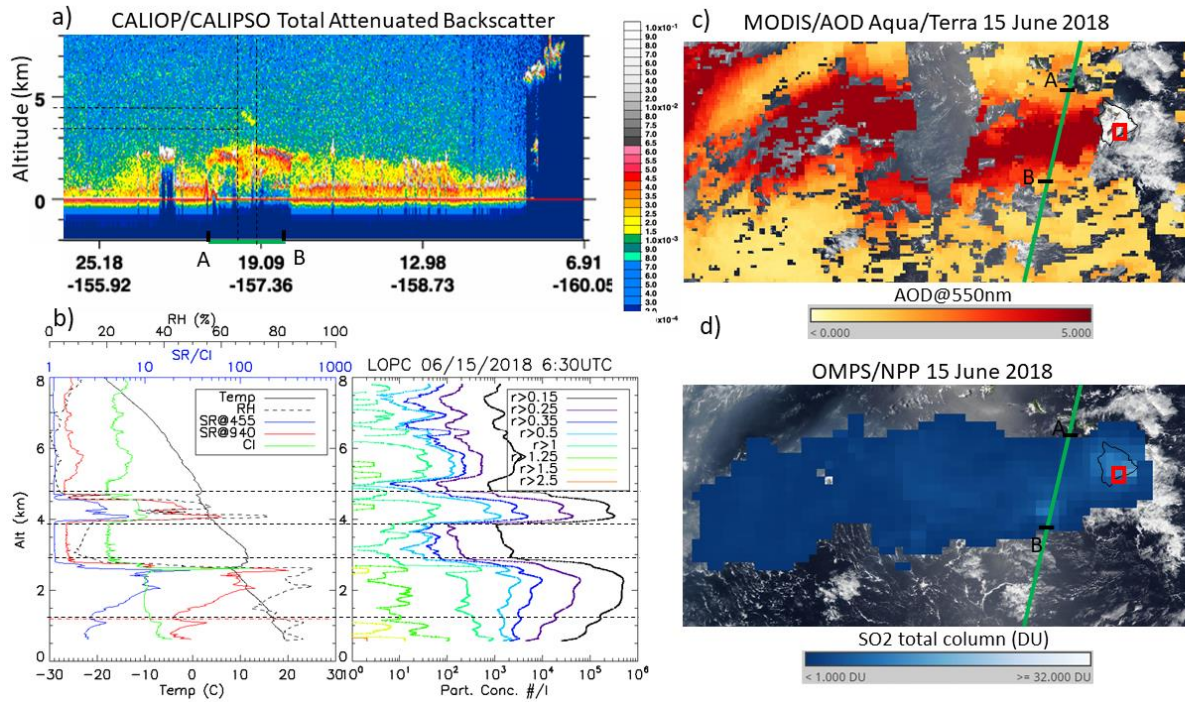*(MODIS) on the Aqua satellite on June, 13th near 23:30 UTC (b) and SO$_2$ mixing ratio derived*

from HYSPLIT between 00:00 and 01:00 UTC on June, 14th. (c&d) Temperature, RH, aerosol

concentration profiles for sizes ranging from 0.15 μm to 5 μm during the ascent and descent of

*the balloon flight (VK02) launched from the Kapapala Ranch (19.263, -155.445) near 1am UTC*

on June, 14th.

8

Figure 9. (a) Total attenuated backscatter from CALIOP/CALIPSO on June, 15th at 12am UTC.

(b) Temperature (Temp), Relative Humidity (RH), aerosol concentration profiles from the

Langley Optical Particle Counter (LOPC) and Scattering Ratios (SR@455nm,SR@940), Color

Index (CI=SR@940/SR@455) from the COBALD backscatter sonde on June 15th launched near

6am UTC. (c&d) MODIS Aerosol Optical Depth from Aqua/Terra and SO2 lower tropospheric

column from OMPS/NPP with the CALIPSO orbit track position shown in green (a). OMPS and

MODIS have been obtained from https://worldview.earthdata.nasa.gov/.

1
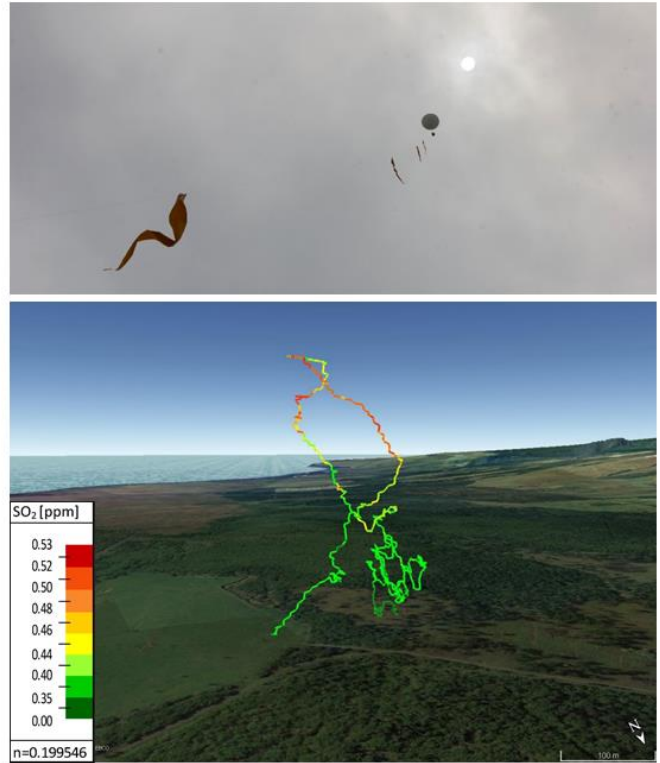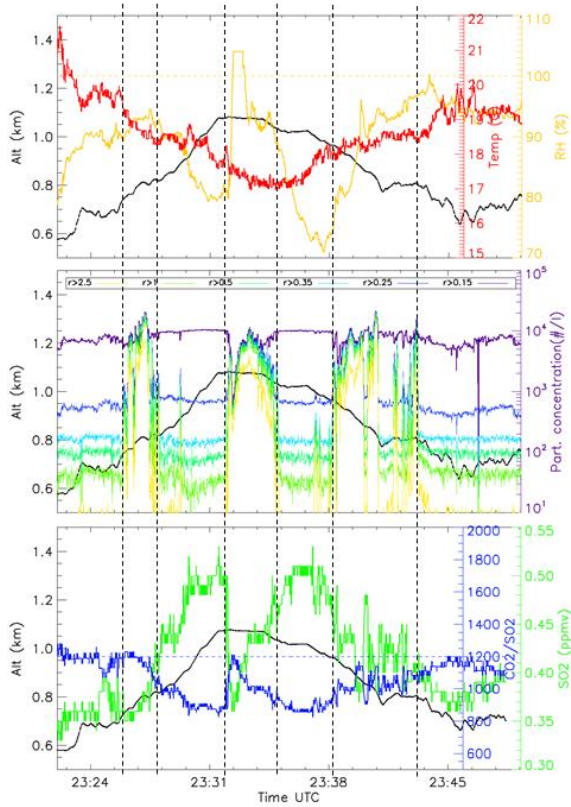
Figure 10. (Right) Upper looking view of the tethered system and balloon position colored with SO$_2$ mixing ratio on Google map. (Left) Time series (from top to bottom) of temperature, RH, GPS altitude, aerosol concentration, SO$_2$ mixing ratio and CO$_2$/SO$_2$ ratio on June, 15th between 23:20 and 23:50 UTC. Aerosol and SO$_2$ concentrations were measured by the ROPC and miniGAS, respectively.

2

3

4

5

6

7

8

9

10

11

1
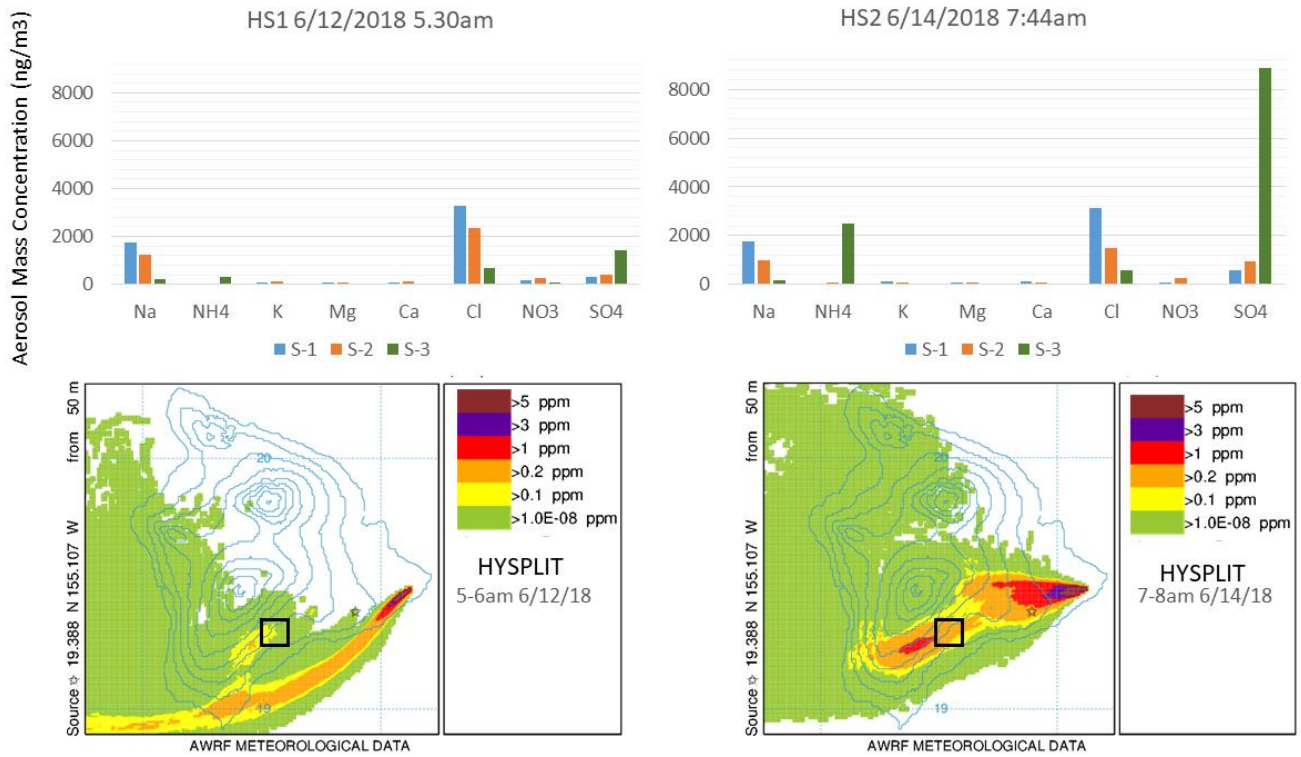
2

3   *Figure 11. (Top) Ionic concentrations from aerosol samples collected on June 12th and 14th*

4   *(Hawaiʻi Sample 1&2; HS1 and HS2) at 5.30 am and 7:44am, respectively. (Bottom) SO₂ mixing*

5   *ratio between 0-100m from HYSPLIT near the time of the sampling.*

6

7

8

9

10

11

Date (UTC)	Location	Time (UTC)	Flight Nb	Flight type	Max Alt	Payloads	Weight	balloon
11-Jun	Kapapala	4am	test	Tethered	100m	ROPC	0.7 kg	300g
13-Jun	Whittingto Beach	3am	VK01	Free Released	28 km	LOPC,ECC,Imet	4.6kg	1200g
14-Jun	Kapapala	1am	VK02	Free Released/Low cut	5km	ROPC,miniGAS,Filter	2 kg	1200g
15-Jun	Kapapala	6am	VK03	Free released	25 km	LOPC,COBALD,ECC	3.5 kg	1200g
15-Jun	Kapapala	11pm	VK04	Tethered	1.2 km	ROPC,miniGAS	2 kg	300g
16-Jun	Kapapala	10pm	VK05	Tethered	1.1 km	LOPC,Impactor, Imet	2.5 kg	1200 g
16-Jun	Kapapala	11pm	VK06	free released	25 km	Imet	0.2g	1200 g
17-Jun	Kapapala	10pm	VK07	Tethered	1.6 km	ROPC,MiniGAS, Impactor	1.2 kg	2000 g
18-Jun	Kapapala	1am	VK08	free released	28 km	LOPC	2.6 kg	2000 g

Table 1. List of balloon flights during the VolKilau campaign together with date, time, location,

flight type, payload, weight and balloon size information. The following acronyms correspond to

ROPC: LASP Light Weight Optical Particle Counter, LOPC: Langley Optical Particle Counter,

ECC: Ozonesonde, Imet: meteorological radiosonde, Impactor (G): Ground samples with the

aerosol impactor, COBALD: backscatter sonde.

1

Con. ng/m^3		Na$^+$	NH4$^+$	K$^+$	Mg^{2+}	Ca^{2+}	Cl-	NO2$^-$	NO3$^-$	SO4^{2-}
HS1 (06/12/2018)	S1	1747	0	0	0	0	3300	0	159	327
5.30am UTC	S2	1249	0	145	0	144	2364	0	245	418
	S3	204	307	0	0	0	674	0	0	1429
HS2 (06/14/2018)	S1	1759	0	122	0	122	3151	0	0	599
7:44am UTC	S2	991	0	0	0	0	1474	0	263	928
	S3	182	2466	0	0	0	577	0	0	8862

2

3   *Table 2. Ionic concentration for the two ground aerosol samples taken during the VolKilau*

4   *campaign on 06/12/2018 and 06/14/2018 at 5.30 am and 7.44am respectively.*